Available online at www.sciencedirect.com
SCIENCE DIRECT
Polymer 47 (2006) 3904–3914
polymer
www.elsevier.com/locate/polymer

Short-term mechanical and structural approaches for the evaluation of polyethylene stress crack resistance

J. Cazenave [a], R. Seguela [b,*], B. Sixou [a], Y. Germain [c]

[a] Groupe d'Etude de Métallurgie Physique et de Physique des Matériaux, INSA de Lyon, Batiment Blaise Pascal, 69621 Villeurbanne, France
[b] Laboratoire Structure et Propriétés de l'Etat Solide, Université de Lille 1, Batiment C6, 59655 Villeneuve d'Ascq, France
[c] Total Petrochemicals Research, Industrial Zone C, Feluy 7181, Belgium

Received 27 January 2006; received in revised form 14 March 2006; accepted 27 March 2006

Abstract

Short-term mechanical behavior together with structural habits at various scale levels of polyethylene are studied in relation to molecular architecture in order to contribute to the understanding of the environmental stress crack resistance (ESCR). Three series of homopolyethylene and ethylene–hexene copolymers issued from 1st and 2nd generation chromium oxide catalysis as well as tandem-reactor Ziegler-Natta catalysis are investigated. Properties are discussed via the incidence on the chain topology of the co-unit concentration and distribution as well as the molar weight distribution. The creep compliance is mainly governed by density, i.e. stiffness. However, at similar density, the three polymers series displays a clear compliance drop that follows the increasing ESCR hierarchy. The natural draw ratio displays monotonous decrease with decreasing density that perfectly parallels the ESCR increase. This property also holds for materials of similar density. The creep compliance and the natural draw ratio are indicators of the macromolecular network strength via the intercrystalline tie molecules. Stepwise isothermal segregation (SIS) allows indirect assessment of the chain fraction that generates a high rate of tie molecules. Correlation is made between SIS and ESCR via the tie molecules that provide strength to the macromolecular network. SIS also enables discriminating polymers of similar density but different molecular architecture. Small-angle X-ray scattering affords quantitative evaluation of the stacking disorder of the semi-crystalline microstructure for which a correlation is established with the crystallization kinetics and the resulting chain topology.

Keywords: Polyethylene; Molecular architecture; Stress cracking

1. Introduction

The use of polyolefins in application domains demanding long life-time in service, such as pipes for gas distribution or fuel tanks for land vehicles, has drastically increased in recent years. The reason is that new generation polyolefins with tailored-cut molecular architecture have much better long-term behavior than their 50-years-old homologues, with very good compromise between stiffness and strength. Investigations for improving the use properties of such materials directly originate from the sustainable development policy, which notably means low energy consumption processing, structure lightening, durability and easy recycling. Polyethylene is much concerned with this topic, more particularly regarding pipe and tank applications [1].

A great problem for evaluating and certificating recent generation PE with respect to life-time is that normalized homologation tests for stress-crack resistance must be conducted for very long times, e.g. several years in the case of the standard pipe pressure test. Even in the case of accelerated tests involving notched samples in surfactant medium, failure may occur after about one month. Quick evaluation methods of new materials would be very useful for producer in order to avoid performing long experiments that will not necessarily have a positive issue. As a corollary, the mechanisms of stress cracking at a molecular scale deserve accurate investigation in order to provide adequate solutions to the problem [2–13].

The phenomenon of slow crack growth is the major process of failure of polyolefins under stress, far below the yield point. It determines the life-time in service. This phenomenon arises from the sporadic nucleation of cavities in the amorphous phase constrained between neighboring crystalline lamella [2,11,13]. Then localized plastic yielding occurs in the proximity of the cavities, accompanied with fragmentation of

* Corresponding author. Tel.: +33 3 20 43 49 13; fax: +33 3 20 43 65 91.
E-mail address: roland.seguela@univ-lille1.fr (R. Seguela).

0032-3861/$ - see front matter © 2006 Elsevier Ltd. All rights reserved.
doi:10.1016/j.polymer.2006.03.094

the crystalline lamellae and partial chain unfolding. This structural transformation of a part of the isotropic material is strictly similar to the so-called fibrillar transition described by Peterlin [14,15] in the case of uniaxial drawing of semi-crystalline polymers. The initial damage gradually grows into a craze, i.e. a crack bridged by numerous microfibrils that prevent crack opening, as nicely demonstrated by transmission and scanning electron microscopy [2–13]. Chemical or physical heterogeneities are suspected to act as nucleating agents for the initial damage. A crack slowly develops from the craze under stress, and propagates through the bulk till the material failure. Brown and collaborators have extensively studied the slow crack growth phenomenon [16–21] in order to (1) understand the mechanisms of crack opening and growth and (2) establish a constitutive law that could help users for predictive purpose. Both molecular and phenomenological aspects have been considered.

The resistance to stress cracking is generally ascribed to the mechanical resistance of the craze microfibrils. It is also assumed that this resistance is governed by the molecular links between the crystal blocks of the microfibrils consisting of intercrystalline tie molecules and chain entanglements: the greater the tie molecules and entanglement density, the higher the stress crack resistance. As a general trend, broadening the molar weight distribution on the high molar weight side and copolymerization are two efficient ways for improving the tie chain concentration. The first way is, however, prejudicial for processing while the second one reduces crystallinity and stiffness. Benefiting from several available catalysis methods, attempts have been made for combining the two ways in order to preserve the best compromise between long-term mechanical behavior, stiffness and process ability.

In the search of a quick evaluation method, it has been shown that samples drawn beyond the yield point may usefully simulate the mechanical behavior of the crack tip microfibrils. Capaccio et al. [22,23] reported creep rate studies that provided good correlation with ESCR: the higher the ESCR of the materials, the lower the creep rate deceleration. Lagaron et al. [24] have carried out direct measurement of the stress borne by the intercrystalline tie molecules via Raman spectroscopy: materials with high ESCR performances displayed reduced stress on individual chains. This latter finding can be taken as evidence of a greater tie chain concentration that involves a better efficiency of the macromolecular network for dispatching the macroscopic stress throughout the bulk material. Although elegant, these methods proved to be unable to discriminate materials of very high rank in life-time scale.

The present paper is a contribution to the understanding of the long-term behavior of polyethylene and related copolymers via structural approaches at various scale levels together with short-term mechanical properties. Environmental stress cracking, creep compliance, natural draw ratio, stepwise crystallization segregation, small-angle X-ray scattering and surface free energy are used in combination. The understanding of the role of every molecular factor on the compromise between stiffness and strength is also an objective of the study. Another goal is to put forward quick evaluation methods for the long-term mechanical behavior.

2. Experimental

2.1. Materials

The polymers of this study consist of high density polyethylene homopolymers and ethylene–hexene copolymers produced from various synthesis methods, namely 1st generation chromium oxide catalysis, 2nd generation chromium oxide catalysis and tandem-reactor Ziegler-Natta catalysis. These blow-molding grade polymers have different molar weight distributions as well as different hexene co-unit concentrations and distributions. The materials and their molecular characteristics were supplied by Total Petrochemicals.

All polymers contain antioxidant and processing aids in weight concentrations of about 1 and 2‰, respectively.

The materials have been compression-molded from pellets into 2 mm thick sheets after being melted for 10 min at 190 °C. Crystallization was achieved by cooling down to room temperature (RT) at about 10 °C/min. Compression-molding has been chosen to impart a homogenous and isotropic reference state to the materials in order to restrict the study to the evaluation of intrinsic properties, irrespective of processing conditions.

2.2. Molecular and physical characterization

The number-average, M_n, weight-average, M_w, and z-average, M_z, molar weights were determined by size exclusion chromatography, using trichlorobenzene as solvent at 135 °C. Molar weight determinations are based on a universal calibration curve. More details on experimental parameters have been reported elsewhere [25].

The hexene co-unit concentration, ξ, was assessed from the methyl group content measured by ^{1}H nuclear magnetic resonance, in consideration of the methyl and vinyl chain ends.

The density, ρ, was measured in a water–alcohol gradient column calibrated with floating glass beads having well-known densities at 23 °C. The standard deviation of the measurements was about 10^{-3}.

Melt flow index was determined at 190 °C under a 2.16 kg load according to the standard method (D1238 ASTM Norm).

2.3. Thermal behavior and crystallization

The thermal behavior of the materials was investigated on a Perkin–Elmer DSC7 calorimeter using samples of about 6 mg. The temperature and heat flow scales were calibrated owing to the melting curves of 99% pure indium and tin samples. The melting point, T_m, was determined from the peak of the melting endotherm of samples crystallized by cooling from 210 °C down to RT at 10 °C/min. The crystal weight fraction, X_c, was assessed from the ratio of the melting enthalpy of the materials to that of a perfect PE crystal, i.e. $\Delta H_m^0 = 270$ J/g

[26]. The crystal volume fraction, ϕ_c, was computed from the relation $\phi_c = X_c\ \rho/\rho_c$, where $\rho_c = 1.000\ g/cm^3$ is the density of the PE perfect crystal [27].

The surface free energy, σ_e, of the chain-folded surfaces of the crystallites has been computed from the Gibbs–Thomson relation [28]

$$T_m = T_m^0\left[1 - \frac{2\sigma_e}{\left(\rho_c L_c \Delta H_m^0\right)}\right] \quad (1)$$

where $T_m^0 = 141.4\ ^\circ C$ is the melting temperature of the PE perfect crystal. The determination of the crystal lamella thickness, L_c, is described below.

Crystallization has been investigated using the stepwise isothermal segregation (SIS) method, with a two-step procedure [29,30]. After several trials for checking the effect of both temperature and duration of the isothermal crystallization, the following conditions were fixed: after melting at 210 °C for 10 min, the material was rapidly cooled down to 120 °C for isothermal crystallization during 4 h. Then, the material was cooled down to room RT at cooling rate of 10 °/min in order to crystallize the remaining crystallizable part. The melting was subsequently recorded by heating at 10 °C/min. Most of the materials displayed two melting peaks corresponding to two polymer species that crystallized during each of the two steps. Three SIS analyses with different samples have been performed for every material. More details on the experimental procedure are given in the 'segregation crystallization' section.

2.4. Structural analysis

Small-angle X-ray scattering (SAXS) experiments were carried out on a laboratory bench equipped with a two-dimensional CCD camera from Roper Scientific. The Cu Kα radiation was selected from a Rigaku rotating anode and collimated owing to a specific point-focusing Goebel mirror from Xenocs. The patterns were corrected for the background scattering and for the geometry and intensity distortions of the CCD detector. The Lorentz-corrected intensity profiles from isotropic samples were plotted as a function of the scattering vector, $q = 4\pi\sin\theta/\lambda$, after azimuthal integration of the patterns over 360°.

The most probable long period of the crystal-amorphous lamellar stacking, L_p, was determined from the precise location of the scattering peak, q_{peak}, via a parabolic fitting, and using the Bragg relation

$$L_p = \frac{2\pi}{q_{peak}} \quad (2)$$

The crystal and amorphous lamella thicknesses, L_c and L_a, were computed from the following relations

$$L_c = \phi_c L_p \quad \text{and} \quad L_a = L_p - L_c \quad (3)$$

assuming a much larger lateral extent of both kinds of lamellae as compared to their thickness.

A more sophisticated analysis of the lamellar stacking regularity in the materials has been checked owing to a modified Hosemann's paracrystalline model [31] that predicts the SAXS behavior of a uni-dimensional stacking of two kinds of layers having different electron densities, namely amorphous and crystalline lamellae. In addition to the number N of lamellar elements diffusing coherently, the parameters of the model consist in the thickness distribution of each lamella population [32,33] that is assumed to obey a Reinhold distribution function [34]: the parameters γ_c and γ_a control both the breadth and skew of the crystalline and amorphous lamella thickness distributions, respectively. The relevant equations for an easy computing of the SAXS intensity profiles are detailed in Refs. [32] and [33]. The paracrystalline parameters of the model are determined by fitting the theoretical scattering intensity curves to the corresponding experimental profiles.

2.5. Mechanical properties

The environmental stress cracking resistance, ESCR, was assessed according to the standard Bell-test [D1693 ASTM Norm] which consists in clamping a rectangular piece of material into bend position in order to activate stress cracking in the more strained region. Ten pieces of every material were tested simultaneously in an environmental medium of pure Igepal, at RT. ESCR data were assessed at the time when 50% of the specimens displayed a visible crack at naked eye. Considering that ESCR may be affected by additives as well as processing conditions, these factors have been kept identical for all the materials in order to make ESCR data relevant to molecular architecture only.

Uniaxial tensile drawing experiments were performed on a MTS machine, at RT, in order to determine the secant modulus at 2% strain. The samples of gauge length 24 mm were drawn up to the yield point at a crosshead speed of 10 cm/min. All the data are average values from 10 measurements. Similar samples were also drawn beyond the yield point for determining the natural draw ratio, NDR. The neck was propagated over a constant distance of 5 cm at a crosshead speed of 10 cm/min. The NDR was determined before unloading from the reduction of the sample cross section, assuming negligible volume variation. This procedure allows more rapid and precise determination of NDR than any direct longitudinal measurement. The reported data are average values from three specimens.

Tensile short-term creep was also studied on isotropic samples at RT, using the same MTS testing machine. The compliance was computed from the ratio of the strain to the applied stress after 15 min creep. All compliance data are average values of three measurements. Details on the experimental method have already been reported elsewhere [35].

Both creep and NDR data are strongly sensitive to preparation conditions so that much precaution should be taken in case of comparison with literature data.

3. Results and discussion

3.1. Molecular and physical characteristics

The polymers investigated in this work are listed in Table 1. The three PE series are labeled as: Cr1X, for the 1st generation chromium-oxide catalysis, Cr2X for the 2nd generation chromium-oxide catalysis and ZNX for the tandem-reactor Ziegler–Natta catalysis. The X digit in the polymer labels indicates the material rank in the decreasing density classification, for every PE series. This classification is roughly connected with the increasing co-unit content. The well known correlation between crystallinity measurements from DSC and density data for polyethylene-based materials is fairly obeyed for the present materials collection. The high rate of rejection of the hexene co-units from the crystal phase, due to severe distortions of the crystal lattice, reduces the crystallization capability of the methylene sequences, as compared with propene co-units for instance [27]. However, the accuracy of the NMR measurements does no allow a precise ranking of the material based on the co-unit content when this latter is below 0.1 mol%.

Comparison of the materials can be made in consideration of the average molar weight data of Table 1. The various PEs are not much different regarding M_n. However, a clear distinction appears between the two Cr series when comparing the M_w data: the polymers of the Cr2 series have a broader molar weight distribution (MWD) that notably extends on the high molar weight side. The M_z values, 2–3 times larger for the Cr2 polymers as compared with the Cr1 ones, corroborate this finding. The presence of a tail of extremely long chains in the MWD of the Cr2 polymers will play a significant role in the mechanical properties. Fig. 1(a) shows schematic plots of the MWD and co-unit distribution (CD) in the Cr1 and Cr2 series that points out the major MWD differences. The monotonic decrease of the co-unit content with increasing MW is a well-known characteristic of ethylene-based polymers from both the chromium oxide and the Ziegler–Natta catalysis [36–38]. It is also worth noticing that co-units are not uniformly distributed along the chains. This is may be a beneficial factor for mechanical strength thanks to intra-molecular crystallization segregation [39].

The differences in MWD and CD between Cr and ZN polymers deserve a specific comment. In contrast to the steadily decreasing co-unit content as a function of increasing molar weight in the Cr polymers (Fig. 1(a)), the ZN polymers have a bimodal MWD due to the tandem-reactor synthesis that produces two chain species (Fig. 1(b)): the lower MW population consists of a homopolymer A whereas the higher MW population consists of a co-unit rich copolymer B. As a consequence, the co-units in the ZN copolymers are preferentially located in longer chain than in the case of Cr copolymers [40–44]. This property of bimodal ZN copolymers, as compared to unimodal Cr copolymers, was previously disclosed by means of a complete molecular analysis of polymer fractions obtained from temperature rising elution fractionation [39].

According to previous studies, the conjunction of high co-unit content and high molar weight is favorable for the generation of intercrystalline tie molecules [16–18,39,44] that play a determining role in the long-term mechanical behavior. The reason is that both crystal-excluded co-units and very long entangled chains hinder the regular folding propensity of flexible methylene chains. At similar density, the Cr2 copolymers have both higher co-unit content and greater amount of long chains, as compared with the Cr1 ones (Table 1). This is a matter of improvement of the long-term mechanical properties of the former polymers. The comparison of the ZN and the Cr2 copolymers is more subtle. Indeed, the latter ones have longer chains than the former ones, as judged from the M_z data, that are favorable for tie chains. But the preferred location of the co-units on longer chains for the ZN copolymers is a matter of increase of the tie chain concentration, as suggested in the previous study dealing

Table 1
Molecular and physical characteristics of the samples: density, ρ; co-unit content, ξ; melt index, MI; number-average, weight-average and z-average molar weights, M_n, M_w, and M_z; crystal weight fraction, X_c; melting point, T_m

Materials	ρ (g/cm^3)	ξ (mol%)	MI (dg/min)	M_n (kDa)	M_w (kDa)	M_z (kDa)	X_c	T_m (°C)
Cr11	0.961	0.0	0.84	15.2	108	730	72.0	136.2
Cr12	0.960	0.0	0.58	16.8	116	940	72.0	135.3
Cr13	0.959	0.0	0.29	18.1	129	950	72.5	136.2
Cr14	0.958	0.0	0.28	14.9	125	920	71.5	135.3
Cr15	0.954	0.2	0.19	19.9	187	2320	67.0	133.6
Cr16	0.951	0.2	0.27	16.7	131	814	65.0	132.8
Cr21	0.959	0.0	0.32	15.0	229	4100	71.0	136.0
Cr22	0.957	0.0	0.19	15.2	203	2190	70.0	134.4
Cr23	0.954	0.1	0.24	19.2	177	1280	66.0	134.7
Cr24	0.954	0.1	0.26	15.4	216	2770	68.0	133.6
Cr25	0.942	0.8	0.20	15.8	187	1770	54.5	128.6
Cr26	0.939	1.2	0.20	16.1	200	2530	50.0	128.1
Cr27	0.938	1.3	0.14	15.4	227	2620	50.5	126.5
Cr28	0.934	1.8	0.13	14.3	231	2770	45.5	126.5
ZN1	0.959	0.1	0.27	13.6	174	1000	70.5	134.4
ZN2	0.954	0.2	0.10	12.6	271	2000	67.0	133.8

For every property, the last digit of the data is relevant to the standard deviation of the measurements.

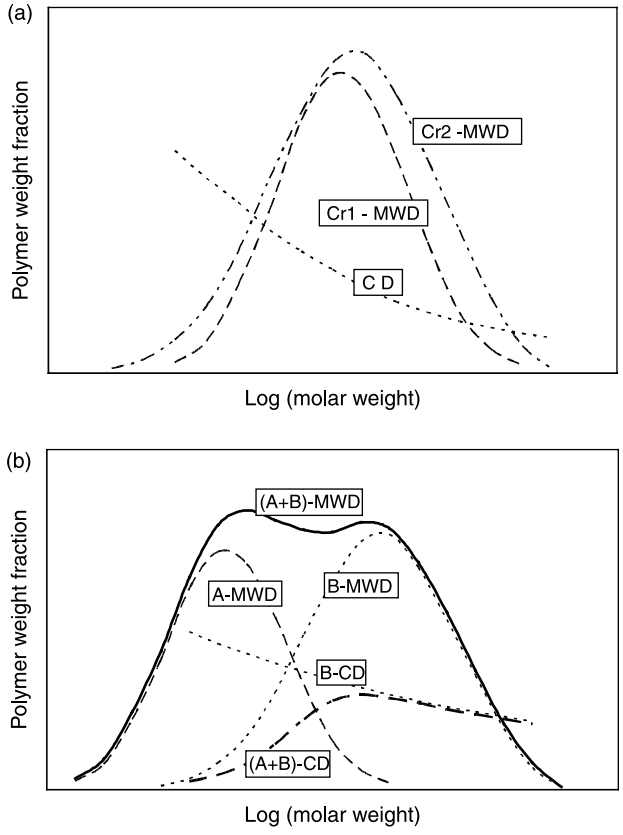

Fig. 1. Schematic molar weight distributions of (a) unimodal Cr and (b) bimodal ZN high density polymers (see text for details).

with a comparison of Cr and ZN copolymers for pipe applications [39]. So, the question 'which of the co-unit distribution or the chain length distribution has a major effect on the tie chain concentration?' is not trivial to answer, especially since the two molecular parameters have detrimental effects on stiffness and processing capabilities, respectively.

3.2. Stress cracking resistance

Fig. 2 shows the ESCR versus density plot for the whole PE collection. For every copolymer series, the ESCR increases with decreasing density. The co-unit concentration increase is most likely responsible for this evolution due to an increasing propensity for generating random chain folding and inter-crystalline tie molecules. In case of materials having similar co-unit concentration, the broadening of the molar weight distribution plays a similar role of promoting intercrystalline tie chains and consequently increasing the ESCR. This point is clearly illustrated through the comparison of Cr23 and Cr24 that have similar density and co-unit concentration. The better stress crack resistance of Cr24 can be ascribed to the significantly higher M_z value.

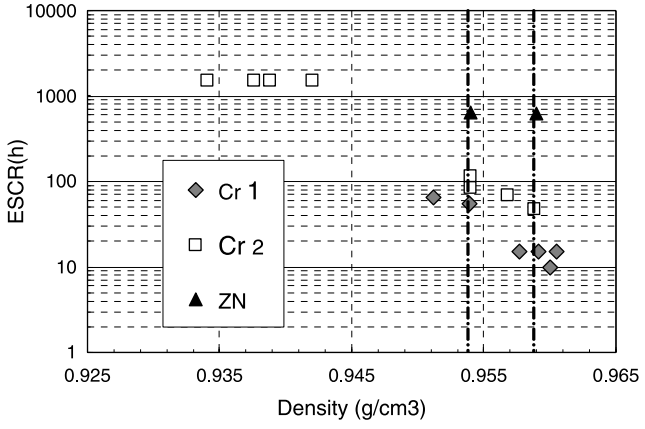

Fig. 2. ESCR versus density for the three polymer series.

It is worth noticing that, from a mechanical standpoint, true tie molecules bridging adjacent crystalline lamellae through the amorphous layer cannot be distinguished from entangled chain loops. Therefore, in the present study, 'tie molecules' embraces the two kinds of intercrystalline molecular linkages.

A much valuable comparison is that of polymers of the three series having similar density, otherwise equivalent crystallinity and very close stiffness. As a mater of fact, one of the challenges in the PE developments for pipe or fuel tank applications is to reach the best compromise between life-time and stiffness. For densities 0.954 and 0.959 g/cm^3, the ESCR increases in the order Cr13 < Cr21 < ZN1 and Cr15 < Cr23 < ZN2, respectively, (Fig. 2). It is obvious that the greater ESCR of the Cr2 copolymers compared with the Cr1 ones is mainly due to greater long chain content. Regarding the comparison between the Cr2 and the ZN copolymers, the preferred co-unit distribution in the longer chains for the latter ones seems to be a major factor of their excellent ESCR performances, in spite of lacking very long chains.

3.3. Creep behavior

Fig. 3 shows the creep compliance versus applied stress for the three series of copolymers. For every PE series, the compliance rigorously increases with decreasing secant modulus. However, the compliance does not obey a strict correlation with density, otherwise with crystallinity.

The creep compliance and the ESCR data also do not display a univocal correlation. This finding seems to contradict the fair correlation previously obtained for a limited number of copolymers having relatively close density but quite different long-term behavior [35]: in that study, the increasing life-time to rupture under constant stress was fairly paralleled by decreasing creep compliance. Therefore, the resistance to stress cracking could be predicted from the resistance to short-term creep. The loss of pertinence of the creep-compliance/ESCR correlation in the present work is due to the relatively broad density range of the copolymers under investigation. Indeed, the modulus drops in parallel with density, involving an increase in creep compliance that does not reveal changes in the tie chain concentration.

Things appear much more interesting when comparing copolymers of the various series at similar density, i.e. equivalent stiffness. Fig. 4 shows that, whatever the applied stress level for copolymers of density 0.954 g/cm^3, the compliance drops in the order Cr15 > Cr23 > ZN2. The same trend can be observed in Fig. 5 for copolymers of density

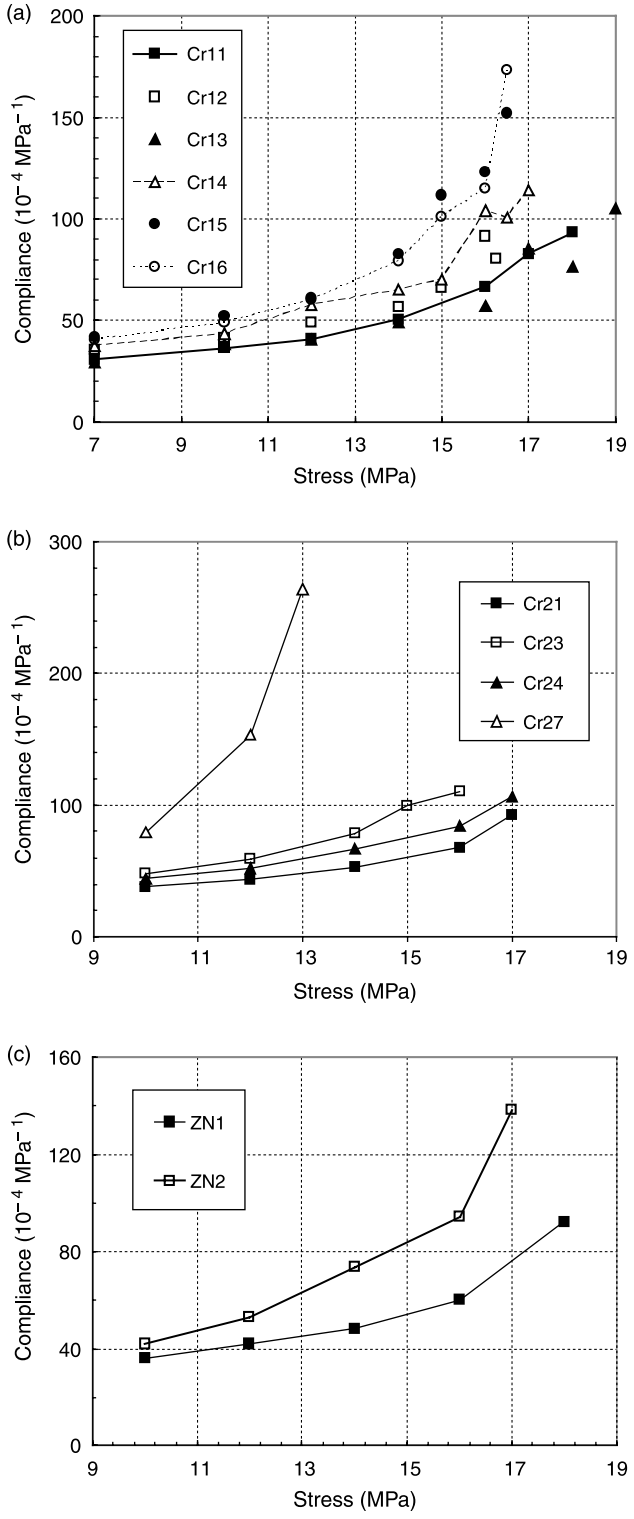

Fig. 3. Creep compliance versus applied stress for polymers of (a) the Cr1 series, (b) the Cr2 series and (c) the ZN series.

0.959 g/cm^3 that follow the decreasing compliance ranking Cr13 > Cr21 > ZN1. Worth noticing is that this compliance ranking conforms to the increasing ESCR ranking, for the two copolymer sets. It means that, at equivalent crystallinity, the combined effect of chain length and co-unit distributions on the chain topology has the same beneficial incidence on creep

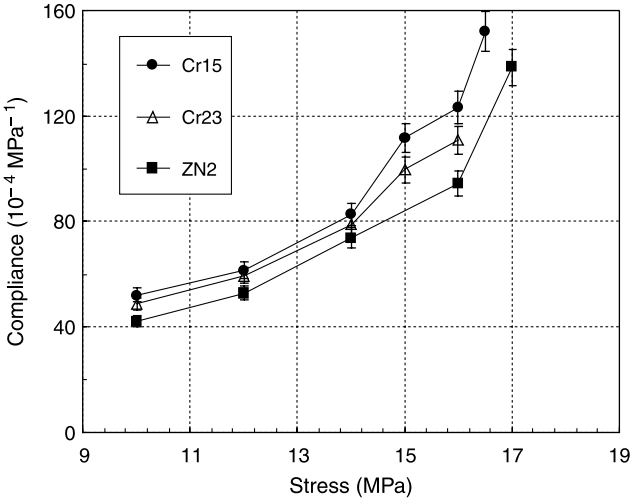

Fig. 4. Creep compliance versus applied stress for the polymers from the three series of similar density 0.954 g/cm^3.

resistance and ESCR. Thus, the creep compliance again displays the previously claimed capability for predicting the long-term behavior of PE, provided that the materials to be compared have about the same density or stiffness. The above findings also reveal that the compromise between stiffness and ESCR gets better in the order Cr1 < Cr2 < ZN.

3.4. Natural draw ratio

The natural draw ratio, NDR, is the plastic strain that spontaneously develops when drawing thermoplastics beyond the yield point. Its physical origin is generally ascribed to the extensibility of the macromolecular network [45]. The situation is not so clear regarding semi-crystalline polymers. According to Peterlin's fibrillar transition model, NDR, results from the chain unfolding at the stage of the lamella fragmentation [14,15]. In this instance, the concentration of random folds and intercrystalline tie chains is a major factor in

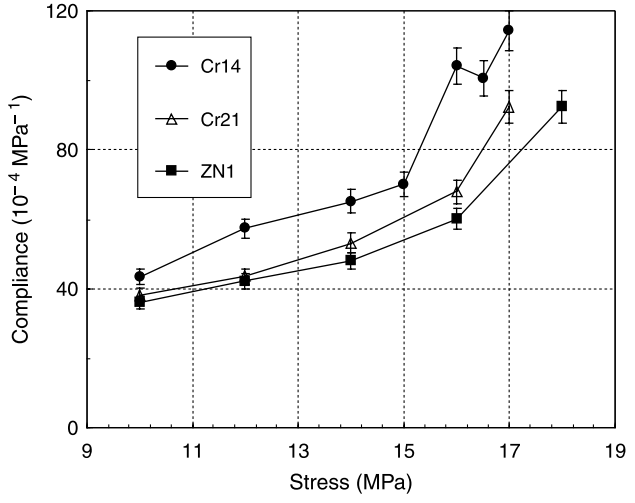

Fig. 5. Creep compliance versus applied stress for the polymers from the three series of similar density 0.959 g/cm^3.

Table 2
Mechanical and structural characteristics of the samples: secant modulus, E; natural draw ratio, λ_n; SAXS long period, L_p; crystal volume fraction, ϕ_c; crystal thickness, L_c; crystal surface free energy, σ_e; thickness distribution parameter, γ; number of coherent scattering lamellae, N

Materials	E (MPa)	λ_n	L_p (nm)	ϕ_c (%)	L_c (nm)	σ_e (J/m^2)	γ	N
Cr11	1060	7.6_0	22.8	69.0	15.8	0.034	0.32	30
Cr12	1050	7.7_0	22.9	69.0	15.8	0.036	0.32	30
Cr13	1100	7.3_5	22.5	70.0	15.7	0.030	0.33	25
Cr14	1050	7.2_0	22.6	68.5	15.5	0.034	0.33	20
Cr15	910	6.8_0	21.6	64.0	13.8	0.043	0.33	20
Cr16	900	6.6_0	20.5	62.5	12.8	0.043	0.35	15
Cr21	1080	6.9_0	23.2	68.0	15.8	0.032	0.32	15
Cr22	990	6.8_0	22.7	67.0	15.2	0.043	0.32	15
Cr23	930	6.7_0	22.6	64.0	14.4	0.040	0.33	10
Cr24	990	6.4_0	21.9	65.0	14.3	0.044	0.33	10
Cr25	610	5.6_0	18.4	52.0	9.5	0.063	0.35	10
Cr26	550	5.5_0	17.7	47.5	8.4	0.063	0.35	10
Cr27	520	5.4_0	17.5	47.0	8.2	0.063	0.36	10
Cr28	470	5.0_0	17.1	43.0	7.3	0.063	0.37	10
ZN1	1020	6.3_5	21.9	68.0	14.9	0.038	0.34	10
ZN2	840	5.8_5	22.2	64.0	14.2	0.043	0.36	10

For every property, the last digit of the data is relevant to the standard deviation of the measurements.

the limitation of lamella fragmentation, and therefore, in the NDR extent, as suggested by Tarin and Thomas [46].

Table 2 reports the NDR data for all the materials of the study. For every series, NDR decreases with decreasing density. The NDR versus density plot of Fig. 6 allows emphasizing the fairly monotonic evolution of the relationship and the very low standard deviation of the data that enables perfect discrimination of the materials. This is thoroughly consistent with the idea that the crystallinity drop due to either co-units [47] or very long chains [48] goes along with a highly disordered chain topology at the crystal surface, namely random chain folding including loose loops and profuse tie chains. As a direct consequence, the capability for lamella fragmentation and chain unfolding is reduced as density decreases, due to the improved macromolecular network strength.

Fig. 6 also allows comparison between materials from the three series at equivalent crystallinity. More particularly, the two sets Cr13–Cr21–ZN1 of density 0.959 g/cm^3 and Cr15–Cr23–ZN2 of density 0.954 g/cm^3 reveal a slight but notwithstanding clear drop of NDR in the order Cr1 > Cr2 > ZN. This finding suggests that the resistance of the macromolecular network to plastic extension increases in the same order.

Interestingly, both the NDR variation with density in every series and the NDR variation between the three series at similar density follow the ESCR hierarchy. Fig. 7 shows that ESCR obeys a univocal relationship with NDR. In every series, the increasing ESCR with decreasing NDR directly reflects the tie chain concentration increase with increasing co-unit content. In the comparison of the three polymer series at similar density, the same ESCR versus NDR relationship emphasizes the determining role of the broad distribution of chain lengths in the Cr2 series and the preferred distribution of the co-units on longer chains in the bimodal ZN series for generating inter-crystalline connections. Whatever their origin, such inter-crystalline tie chains play the same role in stress crack

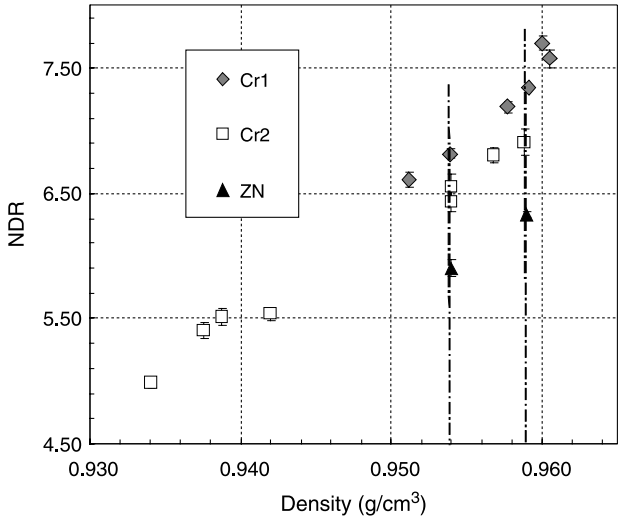

Fig. 6. Natural draw ratio versus density for the three polymer series.

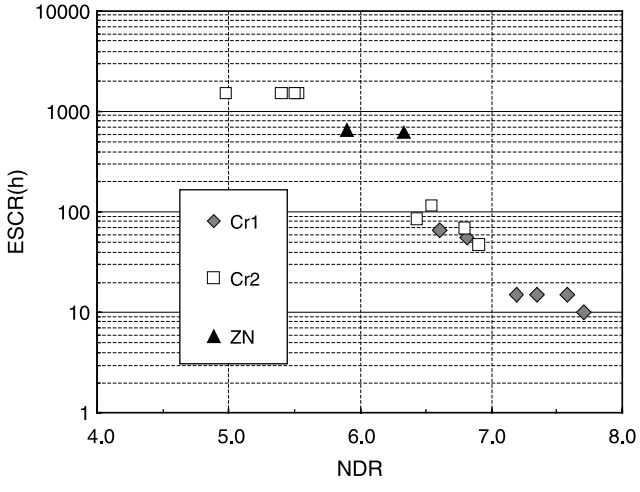

Fig. 7. ESCR versus natural draw ratio for the three polymer series.

resistance and plastic deformation. On the one hand, they delay crack growth during the stress cracking test. On the other hand, they restrict the plastic extension of the macromolecular network during the necking process under tensile drawing.

Last but not the least, the natural draw ratio appears to be a fairly reliable short-term parameter for evaluating the long-term mechanical behavior of HDPE, in consideration of the present data from 16 polymers issued from three different synthesis methods. The reliability of this indicator should be yet confirmed with polymers from other sources.

3.5. Segregation crystallization

Stepwise isothermal segregation (SIS) was used as an indicator of the proportion of polymer species that are able to crystallize at low undercooling under a finite time duration, and those that need large undercooling for growing crystals. The isothermal treatment for 4 h at 124 °C, i.e. moderate undercooling, is performed in order to crystallize the chains species that have the best crystallization capabilities, namely short and medium length chains with very few or without co-units. These chain species are able to form thick crystals in the so-called Regime II, according to Hoffmann designation, which involves a high rate of regular chain folding and few intercrystalline tie chains [49,50]. The slow cooling is carried out for crystallizing the remaining crystallizable part of the materials that was unable to crystallize during the isothermal treatment, due to kinetic factors in relation to chain architecture. These chains species should consist of either co-unit rich chains or very long chain with or without co-units. They are likely to form thinner crystals than the previous ones as a result of the lower temperature at which crystallization occurred during the cooling step. In that case, the crystallization completion should obey Hoffmann's growth Regime III, which means predominant random chain folding with loose loops and profuse intercrystalline tie chains [50,51].

The heating scan recorded after cooling down to room temperature reveals the melting of the two crystal populations, as judged by the occurrence of high temperature (HT) and low temperature (LT) melting peaks. A typical example is shown in Fig. 8. The relative amounts of the two crystal populations can be estimated by a simple separation procedure at the minimum of the double-hump melting endotherm [29], as shown in Fig. 8. The weight fraction of the LT crystal population is called SIS ratio.

SIS ratio data for the whole polymer collection are reported in Fig. 9, as a function of density. The steady increase of the SIS ratio with decreasing density for both Cr1 and Cr2 series reveals an increasing difficulty for HT crystallization due to increasing co-unit concentration. Considering the preferred occurrence of Regime II and Regime III during the two crystallization steps, this finding strongly suggests an increasingly intricate chain topology when density drops. The parallel ESCR increase (Fig. 2) is, therefore, relevant to a favorable chain topology evolution involving numerous intercrystalline tie chains that prevent crack opening under stress.

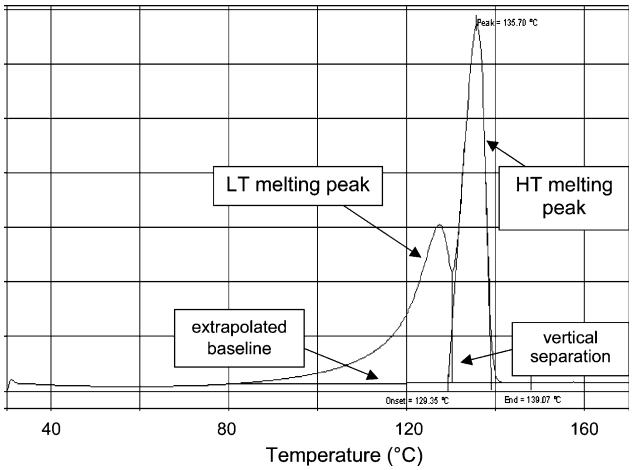

Fig. 8. DSC trace of the Cr16 heating scan after SIS treatment.

It is worth comparing polymers of the three series having similar crystal content, i.e. similar stiffness. The SIS ratio ranking Cr13 < Cr21 < ZN1 and Cr15 < Cr23 < ZN2, for densities 0.959 and 0.954 g/cm^3, respectively, suggests an increasing topological disorder. As already pointed out, the MWD of the Cr2 series is notably broader on the high molar weight side than that of the Cr1 one. This factor is likely to hinder crystallization kinetics and improve the occurrence of tie chain and loose loops in the Cr2 series. Regarding the bimodal ZN materials, preferred co-unit incorporation in long chains is an additional feature in favor of tie chains and loose loops, as compared with the Cr2 and Cr1 series. This conclusion supports the explanation put forward to account for the ESCR increase in the order Cr1 < Cr2 < ZN.

Fig. 10 shows the ESCR versus SIS ratio plot. No univocal correlation appears from this figure in contrast to the NDR versus ESCR plot discussed in the previous section. In spite of its discriminating property, the SIS ratio is less sensitive to the chain topology than the NDR. Nevertheless, it provides structural information on the build up of intercrystalline tie chains.

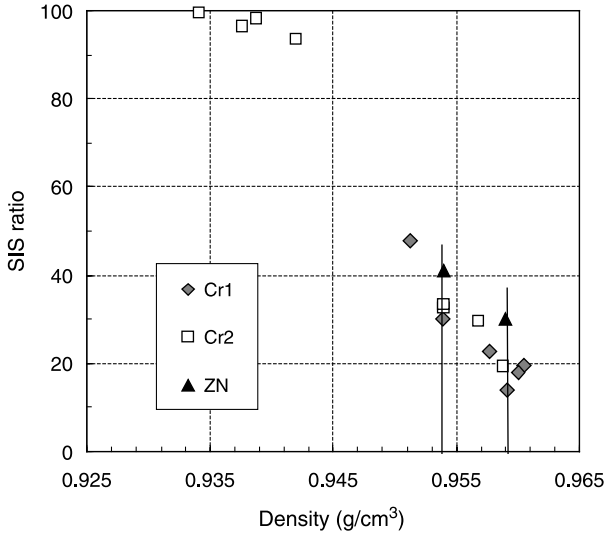

Fig. 9. SIS ratio versus density for the three polymer series.

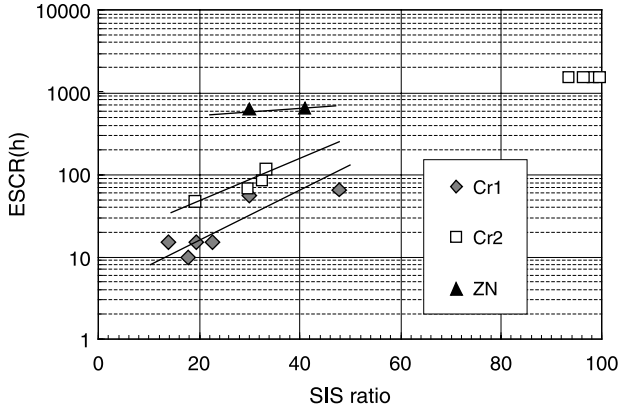

Fig. 10. ESCR versus SIS ratio for the three polymer series.

Although the compression molding of the materials into 2 mm-thick sheets does not involve actual segregation crystallization, one may assume that the variable capability of the investigated materials to generate tie chains remains intact upon slow cooling, due to the intrinsic differences in molecular architecture. Therefore, the topological conclusions drawn from the SIS analysis should apply to the compression-molded samples.

3.6. Small-angle X-ray scattering

The L_p and L_c data are reported in Table 2. For every polymer series, the L_c data display a steady decrease with decreasing density. On the one hand, considering that all polymers have been crystallized following the same slow cooling procedure, this L_c evolution is clearly indicative of an increasing crystallization hindrance. The reason lies either in the co-unit concentration increase or in the molar weight distribution broadening. This is perfectly consistent with the conclusion from the SIS analysis of an increasing trend for Regime III crystallization, involving predominant random chain folding and profuse intercrystalline tie chains. On the other hand, considering Huang–Brown's statistical model of tie chain evaluation [16,18], the lamella thickness decrease is a major factor for generating more intercrystalline molecular connections. These two independent effects converge towards strength improvement with decreasing density of the materials, in agreement with the previous observations of the NDR reduction and ESCR increase.

Comparison of materials at equivalent crystallinity is not so obvious considering the very small L_c variations in the Cr13–Cr21–ZN1 series at 0.954 g/cm^3 and the Cr15–Cr–ZN2 series at 0.959 g/cm^3.

Fig. 11 shows an example of curve fitting of the experimental Lorentz-corrected intensity profile with the paracrystalline model. Analysis of the γ and N parameters of the paracrystalline model provide an additional insight into the structural perfection. In spite of a stepwise evolution of both parameters, the N decrease and γ increase with decreasing density indicate an increasing disorder of the lamellar stacking. It is also worth examining polymers of the three series, at

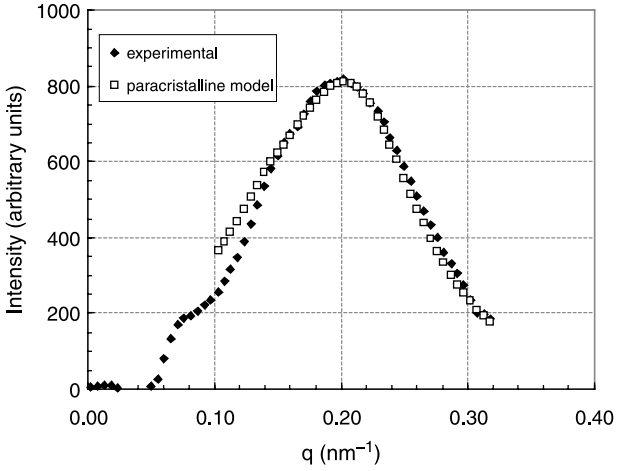

Fig. 11. SAXS intensity profile and curve fitting of the paracrystalline model in the case of the Cr11 polymer.

similar density: a global analysis of the N and γ data of Table 2 reveals an increasing stacking disorder in the following ranking Cr1 < Cr2 < ZN that parallels the conclusion from Fig. 10 of an increasing disorder in the chain topology.

Fig. 12 shows the N versus SIS ratio plot for the whole polymer collection. A very fair correlation appears between the structural disorder represented by N and the SIS ratio which stand for the topological disorder. The lower is the propensity for crystallizing at low undercooling, i.e. high SIS ratio, the lower is the stacking order, i.e. low N values. In parallel, the lamella thickness distributions broaden with increasing SIS ratio.

Considering that low undercooling crystallization promotes regular chain folding together with thick and long crystals that are more stacking-prone than small crystals, the increasing disorder of the lamellar stacking can be taken as a direct consequence of the increasing trend for random chain folding accompanied with profuse tie molecules.

The above correlations between the topological and the structural disorder, for polymers of various density in the same series as well as polymers of similar density in the various

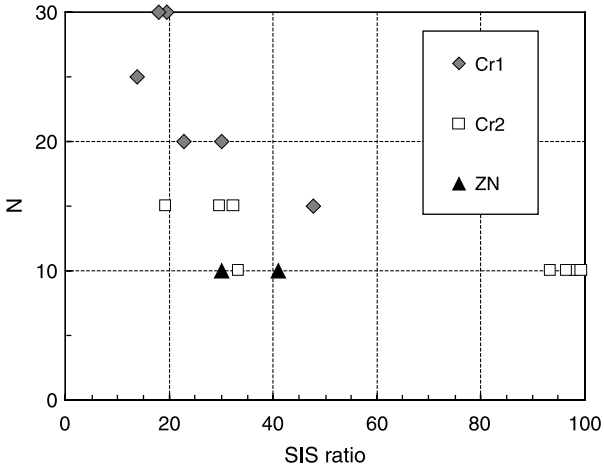

Fig. 12. N versus SIS ratio for the three polymer series.

series, reinforces the point of view that any factor hindering crystallization is beneficial for mechanical properties. In the first instance, the benefit in long-term mechanical behavior is concomitant to a crystallinity reduction that is detrimental for stiffness. This latter point may be yet overcome owing to judicious combination of architectural parameters that allow optimizing the stiffness/durability compromise: as a mater of fact, the peculiar co-unit distribution that can be designed via the cascade-reactor ZN catalysis provides an optimum tie chain concentration without prejudice for stiffness.

3.7. Surface free energy

The surface energy of the chain-folded surface of the crystalline lamellae computed from the Gibbs–Thomson equation and using the L_c data from SAXS are reported in Table 2. In spite of the relatively large standard deviation of the data due to cumulating experimental errors on melting point, SAXS long period and crystallinity, the general trend is that σ_e increases with decreasing density. This trend already reported for ethylene copolymers in a wide range of crystallinity [52,53] is relevant to an increasing topological disorder at the crystal–amorphous interface. As a matter of fact, σ_e for PE-based materials is minimum in the case of chain-folded single crystals and maximum in the case of fringed-micelle crystals. The present findings reveal an increasing content of loose loops and intercrystalline tie chains with decreasing crystallinity, due to either co-unit rejection from the crystal in the case of co-unit rich chains or strong hindrance to regular folding in the case of deeply entangled very long chains. This corroborates the interpretation given above for the evolution of the stacking disorder as a function of density.

The crystal surface free energy is plotted in Fig. 13 as a function of the SIS ratio. Although the data dispersion does not lead to a strictly univocal relationship, the roughly monotonic evolution emphasizes the capability of the two parameters to provide parallel information on the changes of topological disorder as a function of molecular architecture. It is worth noticing that any increase in surface free energy directly parallels an increase in stacking disorder (see γ and N values in Table 2). This is indicative of an increase of crystalline lamella roughness that makes more difficult the regular stacking of the growing lamellae during crystallization.

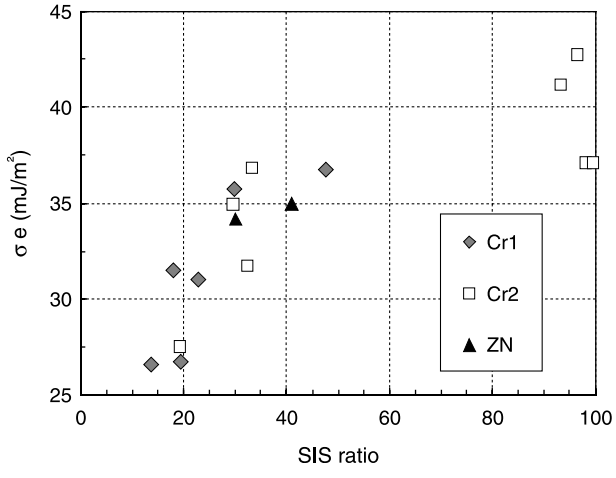

Fig. 13. Surface free energy of the crystal lamella fold surface versus SIS ratio for the three polymer series.

4. Conclusion

The somewhat puzzling short-term creep behavior of the polymers of this study is due to the fact that creep compliance at high loading is a complex combination of stiffness from the crystal phase and strength from the macromolecular network. Comparison at equivalent crystallinity enables focusing on the network strength contribution that develops via the stretching of the intercrystalline tie chains under loading. The issue of the comparison is: the higher the ESCR, the lower the compliance. This is all the more remarkable that Young's modulus, which is just the inverse compliance at very low load, exhibit not any correlation with ESCR.

The natural draw ratio displays a much clearer evolution than the creep compliance. It applies without restriction to all the materials of the study. The natural draw ratio is indeed much sensitive to crystallinity changes but not to the concomitant changes in material stiffness, for every polymer series. The NDR decrease in parallel to the ESCR increase reveals the determining role of the macromolecular network strength in the plastic drawing of the materials beyond the yield point, irrespective of stiffness. At equivalent crystallinity, NDR rigorously follows the ESCR ranking, bringing thus additional support to the determining role of the macromolecular network strength.

Segregation crystallization proved to be a very convenient means for evaluating the amount of polymer chains that cannot crystallize at low undercooling. These chain species are precisely the ones most prone to generating a disordered chain topology with a high content of intercrystalline tie chains and random folds. Surface free energy measurements thoroughly corroborate the topological disorder brought about by such chain species. SAXS revealed a concomitant structural disorder at the scale of lamellar stacking indicating that the disorder in the chain topology at the lamella surface has a detrimental effect on the materials capability for growing large and smooth crystal lamellae.

The structural disorder at various scale levels systematically goes along with an ESCR increase. This correlation can be ascribed to the molecular architecture that governs the build up of the chain topology during the crystallization stage.

Both stepwise segregation crystallization and natural draw ratio proved to be relevant short-term indicators of the long-term behavior that can be used for predictive purpose. The peculiarly high discriminating potential of the natural draw ratio makes it a universal predictive parameter for long-term mechanical behavior of PE-based materials. SAXS stacking disorder and crystal surface free energy only display a rough trend of evolution in relation to ESCR but they both provide quite instructive hints about the incidence of molecular architecture on the development of the structural organization and the chain topology during crystallization.

The concluding comment that could be made about the incidence of HDPE molecular architecture on mechanical properties is that any molecular parameter hindering HDPE crystallization involves a structural disorder at various scale level that goes along with improved long-term mechanical behavior. Long chains are favorable to long-term properties. However, preferred incorporation of co-units in long chains is particularly benefiting for stress-cracking. Co-units not only reduce regular chain folding but also reduce crystal thickness, a favorable factor for the generation of tie chains as demonstrated by Brown et al. [17,19]. The best comprise between stiffness and long-term behavior is found for ZN copolymers that gather all benefiting molecular parameters for structural disorder without loosing crystal content that is necessary for stiffness.

As a final comment, it is worth noting that all properties investigated in this work are sensitive to processing conditions of the materials which must be the same to allow relevant comparisons. The relevance of the various indicators should be extended to other kinds of materials in order to confirm their universality regarding PE-based polymers.

Acknowledgements

The authors are greatly indebted to Total-Petrochemicals for supplying the materials and providing the molecular characteristics and the ESCR data. Financial support to the project and the PhD fellowship to J. Cazenave are also deeply acknowledged. The authors are indebted to the Agence Nationale de la Recherche Technologique for contribution to the PhD fellowship.

References

[1] Series of International Conferences have been running for more than three decades, at roughly one per year rate: ‘International Gas Research Conferences’, org.: Gas Technology Institute, Des Plaines IL, USA; ‘Plastics Pipes’, org.: Institute of Materials, London, UK; ‘Plastic Pipe Fuel Gas Symposia’, org: Plastics Pipe Institute, Washington, DC, USA; ‘Plastic Fuel Gas Pipe Symposium’, org.: American Gas Association, Washington, DC, USA.
[2] Friedrich K. Adv Polym Sci 1983;52/53:225–73.
[3] Lustiger A, Markam RL. Polymer 1983;24:1647–54.
[4] Battacharya SK, Brown N. J Mater Sci 1984;19:2519–32.
[5] Lustiger A, Corneliussen RD. J Mater Sci 1987;22:2470–6.
[6] Narisawa Z, Ishikawa M. Adv Polym Sci 1990;91/92:354–91.
[7] Plummer CJG, Kausch H-H. Macromol Chem Phys 1996;197:2047–63.
[8] Shah A, Stepanov EV, Capaccio G, Hiltner A, Baer E. J Polym Sci, Polym Phys 1998;36:2355–69.
[9] Shah A, Klein M, Stepanov EV, Hiltner A, Baer E. J Mater Sci 1998;33:3313–9.
[10] Kausch H-H, Gensler R, Grein C, Plummer CJG, Scaramuzzino P. J Macromol Sci Phys 1999;B38:803–15.
[11] Plummer CJG, Goldberg A, Ghanem A. Polymer 2001;42:9551–64.
[12] Hamouda HBH, Simoes-Betbeder M, Grillon F, Blouet P, Billon N, Piques R. Polymer 2001;42:5425–37.
[13] Plummer CJG. Adv Polym Sci 2004;169:75–119.
[14] Peterlin A, Corneliussen R. J Polym Sci, Polym Phys 1968;6:1273–82.
[15] Peterlin A, Meinel G. Makromol Chem 1971;142:227–40.
[16] Huang Y-L, Brown N. J Mater Sci 1988;23:3648–55.
[17] Huang Y-L, Brown N. J Polym Sci, Polym Phys 1990;28:2007–21.
[18] Huang Y-L, Brown N. J Polym Sci, Polym Phys 1991;29:129–37.
[19] Lu X, Qian R, Brown N. J Mater Sci 1991;26:917–26.
[20] Zhou Y, Lu X, Zhou Z, Brown N. Polym Eng Sci 1996;36:2101–7.
[21] Lu X, Zhou Z, Brown N. Polym Eng Sci 1997;37:1896–900.
[22] Cawood MJ, Channell AD, Capaccio G. Polymer 1993;34:423–5.
[23] Rose LJ, Channell AD, Frye CJ, Capaccio G. J Appl Polym Sci 1994;54:2119–24.
[24] Laragon JM, Dixon NM, Gerrard DL, Reed W, Kip BJ. Macromolecules 1998;31:5845–52.
[25] Stephenne V, Daoust D, Debras G, Dupire M, Legras R, Michel J. J Appl Polym Sci 2001;82:916–28.
[26] Wunderlich B. Macromolecular physics. Crystal Melting, vol. 3. New York: Academic Press; 1980.
[27] Wunderlich. Macromolecular physics. Crystal Structure, Morphology, Defects, vol. 1. New York: Academic Press; 1973.
[28] Hoffman JD, Davis GT, Lauritzen JI. Treatise on solid state chemistry. In: Hannay NB, editor. Crystalline and Noncrystalline solids, vol. 3. New York: Plenum Press; 1976.
[29] Hosoda S, Uemura A. Polymer J 1992;24:939–49.
[30] Gueugnaut D, Rousselot D. J Appl Polym Sci 1999;73:2103–12.
[31] Hosemann R, Bagchi SN. Direct analysis of diffraction by matter. Amsterdam: North-Holland Publishing Company; 1962.
[32] Hall IH, Mahmoud EA, Carr PD, Geng YD. Colloid Polym Sci 1987;265:383–93.
[33] Annadurai V, Gopalkrishne R, Siddaramaiah R, Somashekar R. Polymer 2000;41:5689–94.
[34] Reinhold C, Fischer EW, Peterlin A. J Appl Phys 1964;35:71–4.
[35] Hubert L, David L, Seguela R, Vigier G, Corfias-Zuccalli C, Germain Y. J Appl Polym Sci 2002;84:2308–17.
[36] Seada S, Suzaka Y. Polym Avd Technol 1995;6:593–601.
[37] Kim Y-M, Park J-K. J Appl Polym Sci 1996;61:2315–25.
[38] Soares JBP, Kim JD, Rempel GL. Ing Eng Chem Res 1997;36:1144–50.
[39] Hubert L, David L, Seguela R, Vigier G, Degoulet C, Germain Y. Polymer 2001;42:8425–34.
[40] Lustiger A, Ishikawa N. J Polym Sci, Polym Phys 1991;29:1047–55.
[41] Berthold J, Böhm LL, Enderle HF, Göbel P, Lüker H, Lecht R, et al. Plast Rubber Compos Process Appl 1996;25:368–72.
[42] Brown N, Lu X, Huang Y, Harrison IP, Ishikawa N. Plast Rubber Compos Process Appl 1992;17:255–8.
[43] Clutton EQ, Rose LJ, Capaccio G. Plast Rubber Compos Process Appl 1998;27:478–82.
[44] Soares JBP, Abbott RF, Kim JD. J Polym Sci, Polym Phys 2000;38:1267–75.
[45] Duckett RA. In: Escaid B, G’Sell C, editors. Plastic Deformation of Amorphous and Semi-Crystalline Materials. Les Ulis, France: Les Editions de Physique; 1982. p. 253–64.
[46] Tarin PM, Thomas EL. Polym Eng Sci 1979;19:1017–22.
[47] Seguela R, Rietsch F. Polymer 1986;27:703–8.
[48] Capaccio G, Ward IM. Polymer 1974;15:233–8.
[49] Hoffman JD, Guttman CM, Di Marzio EA. Faraday Disc Chem Soc 1979;68:177–97.
[50] Hoffman JD. Polymer 1983;24:3–26.
[51] Hoffman JD, Miller RL. Polymer 1997;38:3151–212.
[52] Darras O, Seguela R. Polymer 1993;34:2946–50.
[53] Minick J, Moet A, Hiltner A, Baer E, Chum SP. J Appl Polym Sci 1995;58:1371–84.